

Electrochemical Performance of Li_xSiON Polymer Electrolytes Derived from an Agriculture Waste Product, Rice Hull Ash

Eleni Temeche, Xinyu Zhang, and Richard M. Laine*

Cite This: *ACS Appl. Polym. Mater.* 2021, 3, 2144–2152

Read Online

ACCESS |



Metrics & More



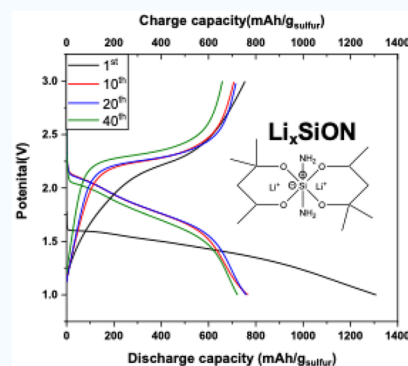
Article Recommendations



Supporting Information

ABSTRACT: The electrochemical performance of Li_xSiON ($x = 2, 4, \text{ and } 6$) polymer electrolytes derived from the agricultural waste, rice hull ash (RHA, 80–90 wt % SiO_2), is reported. Silica can be extracted from RHA by base-catalyzed reaction with hexylene glycol forming the spiroloxane $[(\text{C}_6\text{H}_{12}\text{O}_2)_2\text{Si}, \text{SP}]$ that distills from the reaction solution. Li_xSiON polymer electrolytes form on reacting SP with $x\text{LiNH}_2$, offering a low-cost, low-temperature, and green synthesis route. The effect of N and Li^+ concentrations in the polymer electrolytes are correlated with ionic and electrical conductivity. X-ray photoelectron spectroscopy studies confirm that N and Li contents increase with increasing LiNH_2 content. The amorphous nature and high Li^+ contents of the Li_6SiON electrolyte provide an optimal ionic conductivity (6.5×10^{-6}) at ambient temperature when coated on Celgard. Furthermore, the Li_xSiON polymer electrolytes offer high Li^+ transference numbers ($\sim 0.75\text{--}1$), enabling assembly of Li symmetric cells with high critical current densities (3.75 mA cm^{-2}). Finally, Li-SPAN (sulfurized, carbonized polyacrylonitrile) half-cells with Li_6SiON polymer electrolytes deliver discharge capacities of ~ 765 and 725 mAh/g at 0.25 and 0.5 C rates over 50 cycles.

KEYWORDS: Li_xSiON , polymer precursors, amorphous electrolytes, transference number



1. INTRODUCTION

Lithium ion batteries (LIBs) have been investigated intensively due to their high energy and power densities that enable applications ranging from portable electronics to vehicle electrification.^{1–3} Unfortunately, the flammability of currently used liquid electrolytes and the thermal runaway of traditional LIBs remain as challenges regardless of significant advances in battery management systems (BMS).^{4,5} Thus, solid electrolytes (SEs) are now highly sought due to their high thermal stability, reduced flammability, and resistance to lithium dendrite penetration, potentially enabling new battery designs and chemistries that can enhance both gravimetric and volumetric energy densities.^{6–8} These objectives provide tremendous motivation to synthesize promising SEs with competitive ionic conductivities and wide electrochemical stabilities equal to or surpassing liquid electrolytes.^{7,9,10}

The discovery of LISICON (Li^+ superionic conductors)^{11,12} provided motivation to develop oxysalt $\text{Li}_3\text{PO}_4\text{--Li}_4\text{SiO}_4$ solid solutions targeting and realizing two order magnitude improvements in conductivity (10^{-6} S/cm) compared to single-phased Li_3PO_4 electrolytes (10^{-8} S/cm).¹³ This improvement is attributed to increases in Li interstitial site concentrations.¹⁴ As P^{5+} is partially substituted by Si^{4+} , interstitial Li^+ ions are introduced to the Li_3PO_4 structure.¹⁵ Molecular dynamic simulations of mixed Si/P compositions reveal the formation of a continuous 3D network of Li^+

conduction pathways with a cooperative-type interstitial mechanism.¹³

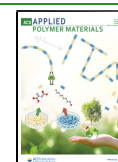
Moreover, studies show that N doping of the O site in Li_3PO_4 promotes faster Li diffusion and improves electrochemical stability attributed to introduction of disorder and decreases in electrostatic energy.^{16,17} The room temperature ionic conductivity of amorphous LiPON ($\sim 3 \times 10^{-6}$) is 2 orders of magnitude greater than Li_3PO_4 .^{18,19} This enhancement is ascribed to the presence of N bridges at high Li^+ contents, which favors the mobility of Li and effectively renders P/O/N immobility.^{17,20}

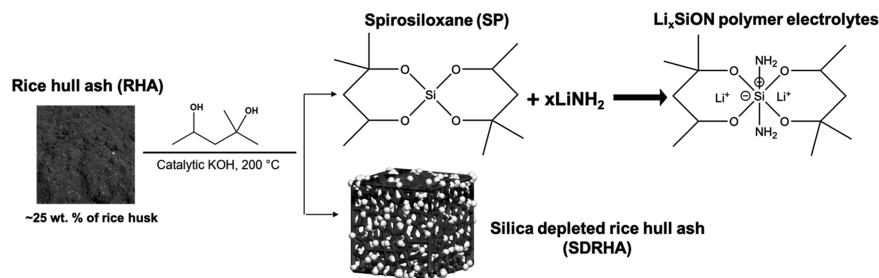
Thus, controlling the nitrogen content is key to achieving a higher ionic conductivity.^{21,22} Both computational and experimental studies have demonstrated that amorphous rather than crystalline LiPON is a better Li conductor attributed to increases in diffusion/conduction due to reduction of overall electrostatic interactions and higher disorder within the material.^{17,20,21,23} Recently, we demonstrated that the introduction of Si into Li_xPON polymer electrolytes enhances ionic conductivity and lowers the activation energy of the

Received: February 8, 2021

Accepted: March 17, 2021

Published: March 30, 2021



Scheme 1. Lithiation of SP to Form Li_xSiON Polymer Electrolytes

polymer electrolyte (Li_xSiPON) by shortening the distance between Li^+ binding sites.^{21,24} With this background, here we investigate the effect of N introduction into amorphous Li_4SiO_4 -like polymer analogs.

Exploration of Li^+ -containing oxynitrides as electrolytes has been limited to thin-film batteries because of their low ionic conductivities ($10^{-6} \text{ S cm}^{-1}$) at ambient temperature.^{4,22,25} In contrast, oxide-based SEs (LATP, LLZO, and LLTO) offer optimal ionic conductivities (0.1–1 mS/cm) at ambient temperature.^{26–29} However, the integration of oxide SEs with high ionic conductivities into the current battery structures remains challenging mainly due to high resistivities at electrode/SE interfaces.^{4,30,31}

Most oxide SEs must be sintered at elevated temperatures to fully densify, form target phases, and reach optimal Li^+ diffusivities.^{4,28,32} This limits the assembly of all solid-state-batteries (ASSBs) as co-sintering electrolytes with electrodes will result in unwanted interfacial layers/defects, phase changes, electrochemistries, and degraded mechanical properties.^{4,31,33} In addition, the ceramics nature (brittleness and stiffness) of oxide-based SEs restrict both their fabrication and operation of ASSBs.⁴ In contrast, amorphous electrolytes advantageously offer both isotropic Li^+ conduction and good interfacial contact with electrodes.³⁴

Assembly of commercially viable ASSBs mandates careful management of both fabrication and material costs especially for SEs. McCloskey et al.³⁵ suggest that SE costs should be $\$10/\text{m}^2$ to compete with conventional LIBs. In this light, we recently developed a novel, amorphous polymer electrolyte, Li_xSiON , derived from rice hull ash (RHA), an agricultural waste product.³⁶

Scheme 1 illustrates the extraction of silica from RHA by simple distillation of spiro-siloxane, [$\text{SP} = (\text{C}_6\text{H}_{12}\text{O}_2)_2\text{Si}$]. Li_xSiON ($x = 2, 4, \text{ and } 6$) polymers with varying Li and N contents can be synthesized simply by reacting SP with $x\text{LiNH}_2$, offering a low-cost, low-temperature, and green synthesis route.³⁶

In this work, we characterize the physical and electrochemical properties of Li_xSiON polymer electrolytes by X-ray diffraction (XRD), X-ray photoelectron spectroscopy (XPS), Fourier transform infrared spectroscopy (FTIR), and electrochemical impedance spectroscopy (EIS) studies. We also correlate compositional and structural changes as a function of nitrogen content and degree of lithiation with ionic conductivities.

Thereafter, we detail the electrochemical stabilities and diffusion kinetics of $\text{Li}/\text{Li}_x\text{SiON}$ polymer electrolyte systems in symmetric cells. The Li_6SiON polymer electrolyte shows optimal ohmic stability at current densities as high as $3.75 \text{ mA h cm}^{-2}$. Coincidentally, we explored transference numbers and electrical conductivities of these polymer electrolytes. The

compatibility of the polymer electrolyte with SPAN (sulfurized, carbonized polyacrylonitrile) cathodes was also investigated.³⁷ The Li -SPAN³⁸ half-cell with the Li_6SiON polymer electrolyte delivered a specific capacity of $\sim 725 \text{ mAh/g}$ over 50 cycles.

2. EXPERIMENTAL SECTION

2.1. Materials. RHA was provided by Wadham Energy LP (Williams, CA). To remove the impurities, RHA was milled in diluted hydrochloric acid (HCl) following the procedures described elsewhere.^{39,40} Lithium amide (LiNH_2) and hexylene glycol (HG) were purchased from Acros Organics (Fair Lawn, NJ). Potassium hydroxide (KOH), lithium metal ($\sim 0.75 \text{ mm}$), HCl, tetrahydrofuran (THF), and *N*-methylpyrrolidone (NMP) were obtained from Sigma-Aldrich (St Louis, MO). Prior to use, THF was distilled from sodium benzophenone ketyl/ N_2 . Coin cell parts and a Celgard 2400 separator ($\sim 25 \mu\text{m}$) were purchased from MTI Corporation (Richmond, CA).

2.2. Syntheses of Li_xSiON Polymer Electrolytes. Detailed discussion about the synthesis and structural composition of the Li_xSiON polymer electrolytes can be found elsewhere.³⁶ In brief, SP was directly distilled out by reacting RHA with HG using a catalytic base at 200 °C. The Li_xSiON polymer precursors were then synthesized by reacting SP with various LiNH_2 contents (Scheme 1) to where the LiNH_2/SP mole ratio is in the range of ~ 2.1 – 6.6 .³⁶ The analytical methods used in this work are provided in the Supporting Information.

2.3. Cell Fabrication. Electrochemical impedance spectroscopy (EIS), cyclic voltammetry (CV), and galvanostatic cycling tests were conducted using an SP-300 potentiostat/galvanostat (Bio-Logic Science Instruments, Knoxville, TN). The total ionic conductivities of the Li_xSiON electrolytes dissolved in THF (0.05 g mL^{-1}) were measured by assembling symmetric cells using a Celgard separator ($18 \text{ mm} \times 25 \mu\text{m}$) and stainless steel (SS) disks ($\phi = 8 \text{ mm}$). Prior to electrochemical characterization, the Li_xSiON polymer electrolyte, Celgard, Li metal, and SPAN electrode ($\phi = 6 \text{ mm}$) were stored in a glovebox (MBRAUN) filled with Ar. For EIS tests, an AC amplitude of 10 mV over a frequency range of 7 MHz to 1 Hz was used. The temperature-dependent ionic conductivities were performed between -10° and 85° C . The electrochemical stability window of the Li_xSiON electrolyte was investigated by conducting cyclic voltammetry (CV) measurements at a scan rate of 1 mVs^{-1} .

Symmetric cells were assembled following the standard procedure described elsewhere.²¹ To evaluate the stability and critical current density, the $\text{Li}/\text{Celgard}+\text{Li}_x\text{SiON}/\text{Li}$ symmetric cells were cycled between ± 0.75 and 3.75 mA cm^{-2} current densities at room temperature. Detailed electrode fabrication procedures for SPAN electrodes can be found elsewhere.^{37,41} The SPAN/Celgard + $\text{Li}_6\text{SiON}/\text{Li}$ half-cell was assembled in 2032 coin cells and charge/discharge between 1 and 3 V at 0.25 and 0.5 C rates.

The Li^+ transference number (t_{Li^+}) of the polymer electrolyte was calculated using eq 1 as suggested by Bruce et al.⁴²

$$t_{\text{Li}^+} = I_{\text{ss}}(U - Z_0 \times I_0) / I_0(U - Z_{\text{ss}} \times I_{\text{ss}}) \quad (1)$$

where I_0 and I_{ss} are the initial and steady-state current values obtained from chronoamperometry measurement, respectively. The initial and

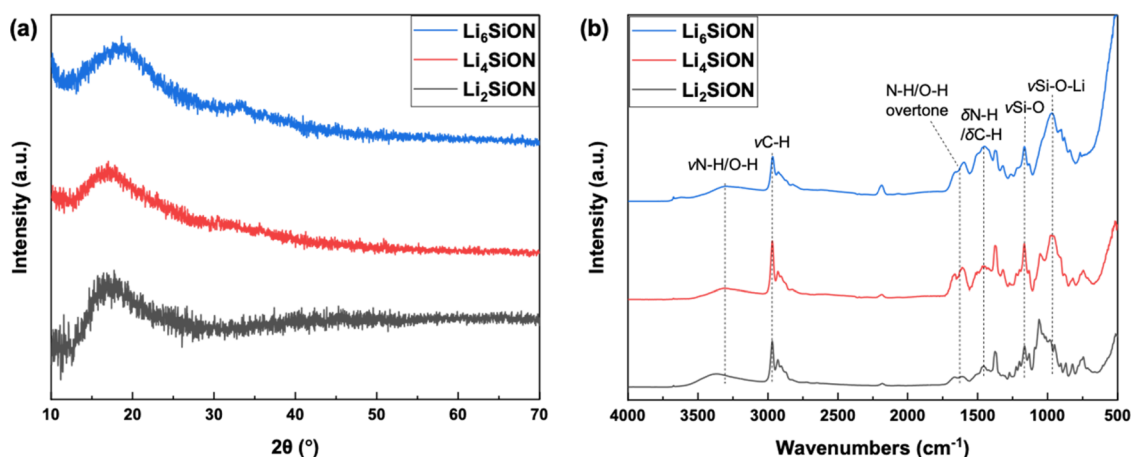


Figure 1. (a) XRD patterns and (b) FTIR spectra of Li_xSiON polymer electrolytes.

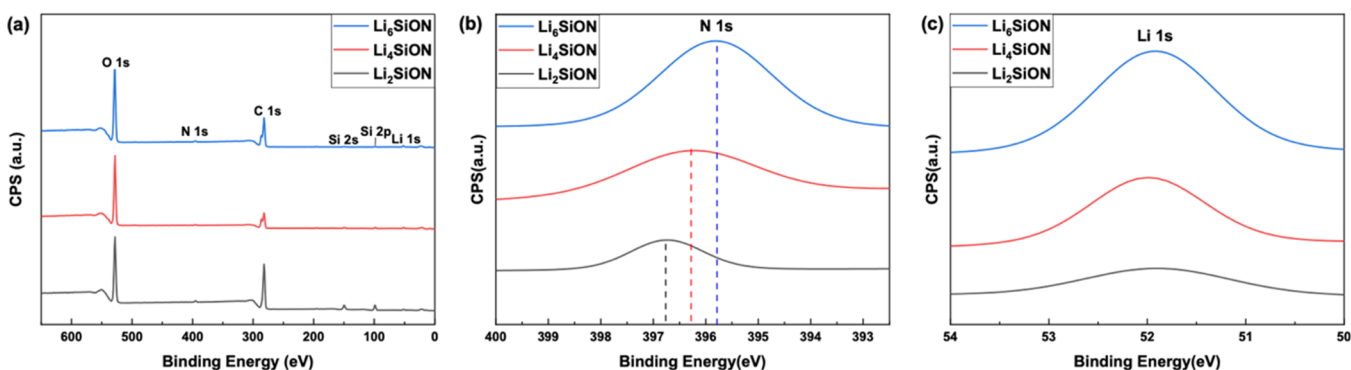


Figure 2. (a) Wide scan XPS spectra, (b) core N 1s, and (c) core Li 1s plots of Li_xSiON polymer electrolytes.

steady-state resistances obtained from EIS studies are represented by Z_0 and Z_{ss} , respectively. U represents the applied potential.

The electrical conductivities (σ_e) of the polymer electrolytes were determined by using eq 2

$$\sigma_e = (t \times I_{ss}) / (A \times U) \quad (2)$$

where the thickness of Celgard is represented by $t = 25 \mu\text{m}$ and A is the area of the electrode ($\phi = 8 \text{ mm}$).

3. RESULTS AND DISCUSSION

In this section, discussion focuses on the structural and surface properties of the Li_xSiON polymer precursors as characterized by XRD, FTIR, and XPS analyses. The second part of the discussion entails the electrochemical performance of the Li_xSiON electrolytes assessed according to ionic conductivity, electrical conductivity, transference number, and the stability of the Li_xSiON electrolyte in symmetric and half-cell configurations.

3.1. Compositional Characterization of Li_xSiON Electrolytes. The Li_xSiON precursors were dried under vacuum/1 h/25 °C to evaporate the solvent (THF). The dried precursors were then compacted into pellets ($\phi = 13 \text{ mm}$) at 10 kpsi/25 °C. Figure 1a shows XRD patterns of the Li_xSiON pellets with broad peaks centered $\sim 20^\circ$ 2θ , indicating an amorphous nature as also seen for amorphous Li_4SiO_4 thin films.^{34,43} Nakagawa et al.³⁴ report that XRD patterns of pulsed laser deposited Li_4SiO_4 thin films also present a broad peak at 20° 2θ , indicating a lack of crystallinity. Amorphous materials often provide improved charge carrier mobility in part by eliminating grain boundaries.²⁵

In Figure 1b, FTIR spectra of the Li_xSiON precursors present broad peaks at $\sim 3400 \text{ cm}^{-1}$ corresponding to $\nu\text{N-H}$, with N-H overtones at 1600 cm^{-1} .³⁶ The peak at $\sim 3000 \text{ cm}^{-1}$ is assigned to $\nu\text{C-H}$. The small peak at $\sim 2250 \text{ cm}^{-1}$ might be CO_2 absorption by the sample due to brief air exposure. The sharp peak at $\sim 1400 \text{ cm}^{-1}$ is attributed to $\delta\text{N-H}/\delta\text{C-H}$. Peaks in the range of $1000\text{--}1200 \text{ cm}^{-1}$ arise from $\nu\text{Si-O}$ bands,³⁴ while peaks at $\sim 900\text{--}1000 \text{ cm}^{-1}$ correspond to $\nu\text{Si-O-Li}$.

Figure 2a shows XPS wide scan surveys revealing signature elements (Li, Si, O, and N). The C peak corresponds to the formation of $\text{LiOH}/\text{Li}_2\text{CO}_3$ on the surface due to brief air exposure, supporting the FTIR data (Figure 1b). Table 1 lists

Table 1. Atomic Ratios of Li_xSiON Polymer Electrolytes Based on XPS Analyses

ratio	Li_2SiON	Li_4SiON	Li_6SiON
Li/Si	1.9	10.8	39.6
Si/N	8.4	3.3	0.85
C/O	2.4	1.3	1.6

the deduced atomic percentage of Li_xSiON precursors dried at RT/1 h/vacuum. The Li/Si and Si/N ratios increase with increasing LiNH_2 content such that the Li_6SiON polymer electrolyte has the highest Li concentration. The N atomic percentage (0.7–0.8) at the surface is much lower than the calculated values (5),³⁶ indicating the loss of N as NH_3 during overnight vacuum treatments prior to XPS studies. The N 1s core spectra (Figure 2b) of Li_xSiON polymer electrolytes show shifts toward lower binding energies with increasing LiNH_2

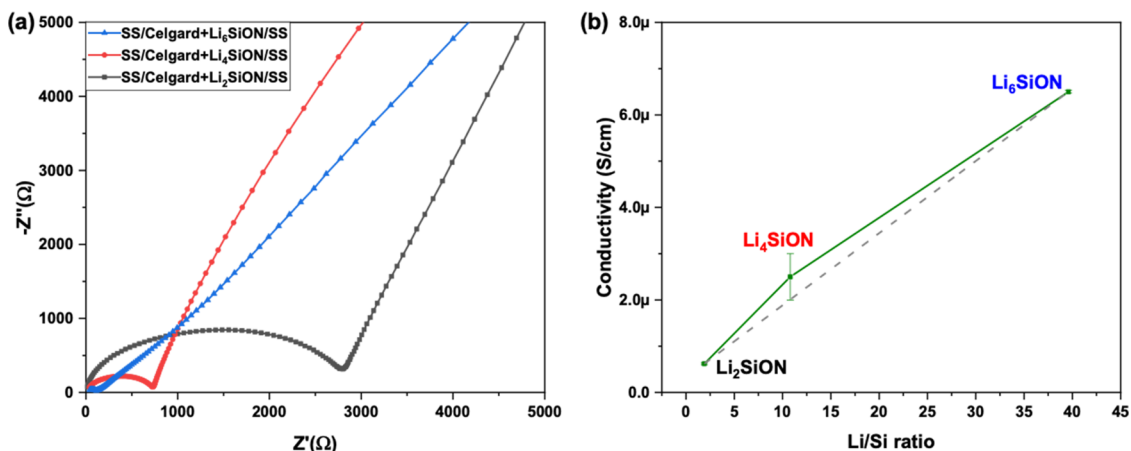


Figure 3. (a) Nyquist plots of SS/Celgard+Li_xSiON/SS symmetric cells and (b) Li/S ratio vs ionic conductivity at ambient temperature.

content. This is attributed to the presence of covalent N–H bonds that increase the electron density around the nitrogen atom.⁴⁴ The Li 1s peak at ~52 eV corresponds to the presence of Li₂O,⁴⁵ and it seems to increase with increasing LiNH₂ content (Figure 2c).

3.2. Electrochemical Characterization of Li_xSiON Electrolytes. Figure 3a presents Nyquist plots of SS/Celgard+Li_xSiON/SS symmetric cells. The total ionic conductivities are calculated similarly to conventional liquid electrolytes-soaked separators. Detailed procedures can be found elsewhere.²¹ Table 2 lists the obtained total ionic

Table 2. Total Ambient Ionic Conductivities of Celgard +Li_xSiON Polymer Electrolytes

polymer electrolytes	conductivity (S/cm)
Li ₂ SiON	$6.2 \pm 0.2 \times 10^{-7}$
Li ₄ SiON	$2.5 \pm 0.5 \times 10^{-6}$
Li ₆ SiON	$6.5 \pm 0.03 \times 10^{-6}$

conductivities of the polymer electrolytes. The Celgard +Li₆SiON polymer electrolyte shows the highest Li⁺ conductivity of $\sim 6.5 \times 10^{-6}$ S/cm at ambient temperature. The ionic conductivity improves by an order of magnitude for Li_xSiON polymer electrolytes, suggesting that increasing the Li content does improve the conductivity.

Studies have shown that the ionic conductivity of Li_xSiPON electrolytes is higher than lithium silicophosphate, attributed to the introduction of N, which presumably reduces electrostatic interactions.^{21,46} However, typically N-doped lithium silicophosphates and lithium phosphates are synthesized using gas-phase deposition techniques, which are costly and require complicated steps to produce thin films, making them challenging for the assembly of ASSBs.^{47–49} In contrast, here we demonstrate a facile polymer precursor route to Li_xSiON electrolytes impregnated on Celgard with optimal ionic conductivity at ambient temperature. Furthermore, our materials are derived from a plentiful agricultural waste (RHA), making them attractive from both a cost and environment-friendly perspective.

One effective method of increasing the ionic conductivity of electrolytes is to increase the charge carrier density and mobility of the charged species. The former is difficult to attain using gas-phase deposition methods, as previously reported by multiple groups,^{50,51} as Li concentrations seem to approach an upper limit of 3, nearly irrespective of the deposition method. Nimisha et al.⁵² report that N₂ flow rate is a key process parameter in gas-phase deposition techniques that governs the ionic conductivity of N-doped thin films. However, increasing the N₂ flow (40 sccm) rate results in a reduction in sputtering rate and a decrease in ionic conductivity of LiPON thin films.⁵² Here, we demonstrate that the ionic conductivity increases

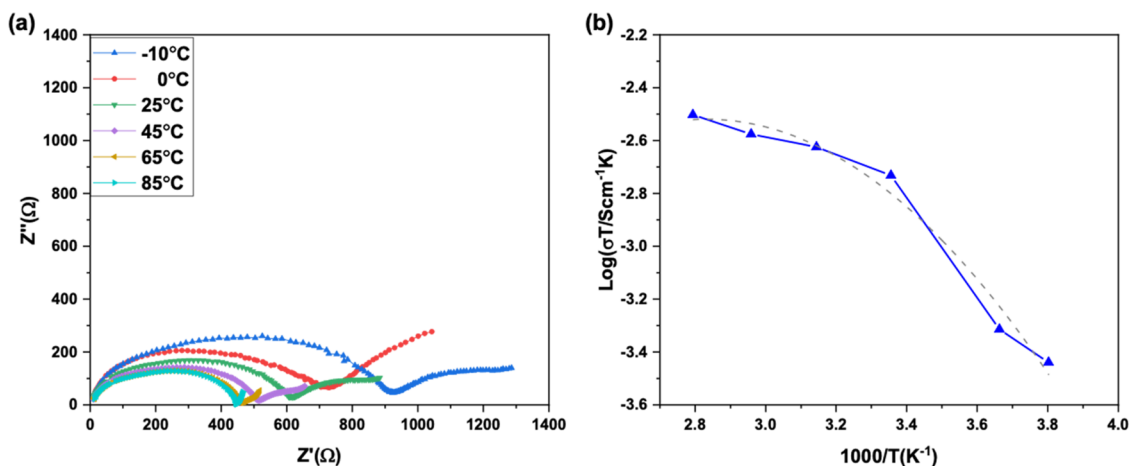


Figure 4. (a) Nyquist and (b) Arrhenius plots of SS/Celgard+Li₆SiON/SS.

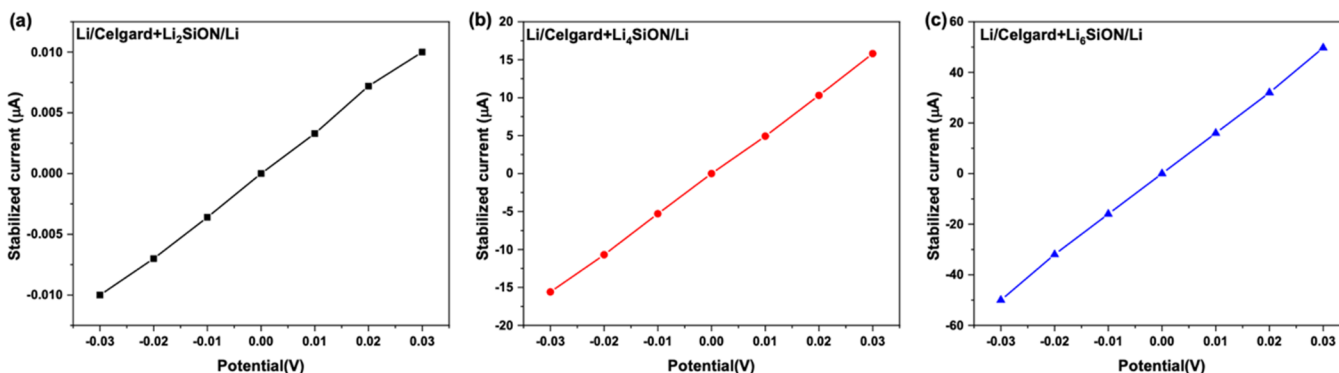


Figure 5. Stabilized current (I_{ss})–voltage (U) relations of Li symmetric cells with (a) Li_2SiON , (b) Li_4SiON , and (c) Li_6SiON electrolytes.

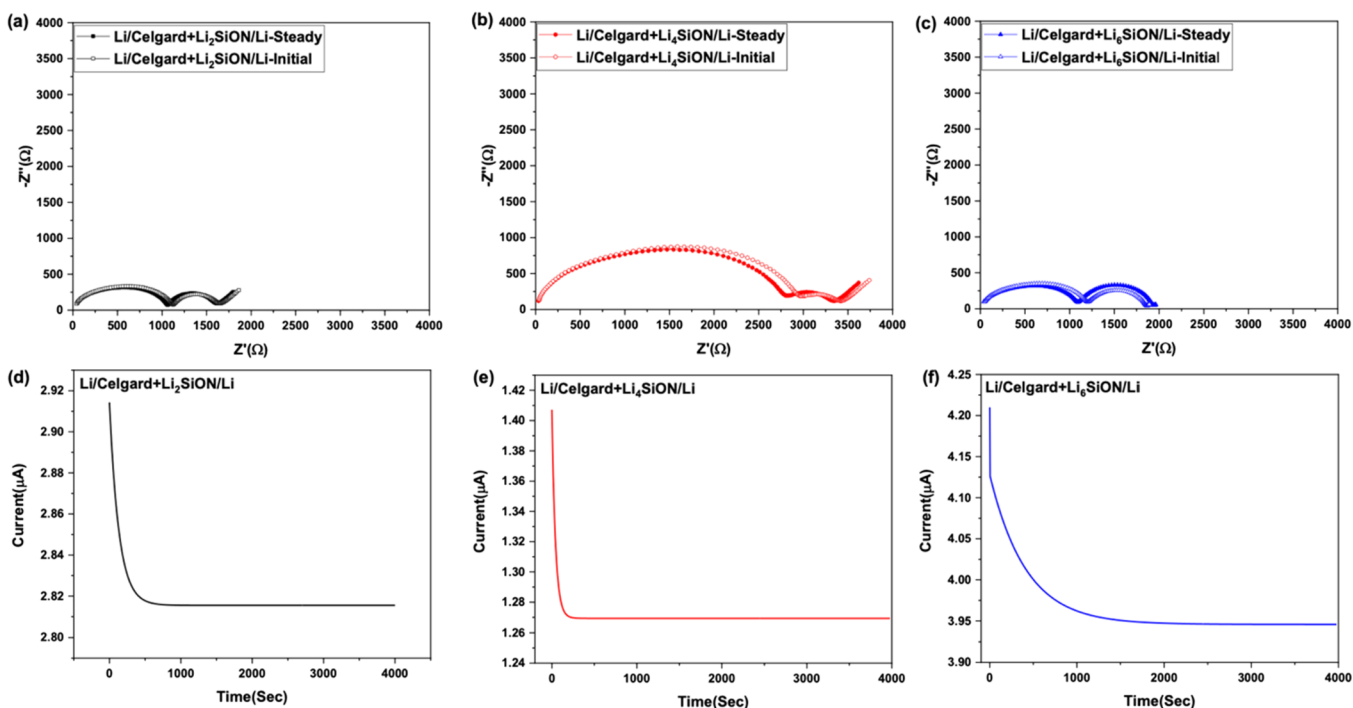


Figure 6. Nyquist (a–c) and chronoamperometry (d–f) plots of Li/Celgard+ Li_xSiON /Li cells.

linearly with Li/Si ratio (Figure 3b). The polymeric route allows control of Li^+ and N concentrations by adjusting initial LiNH_2 amounts.

In addition, the amorphous nature of the polymer electrolyte likely provides isotropic Li^+ conduction, eliminating grain boundary resistivities. Nakagawa et al.³⁴ report that the ionic conductivity of Li_4SiO_4 amorphous films deposited by PLD is $\sim 4 \times 10^{-7}$ S/cm at ambient temperature. The N-doped Li_4SiO_4 polymer electrolyte on Celgard exhibits an order of magnitude higher conductivity compared to the amorphous thin film fabricated by gas-phase deposition techniques.

Figure 4a presents typical Nyquist plots for SS/Celgard+ Li_6SiON /SS cells, where AC impedance measurements were performed from -10° to 85°C . The linear fit to the Arrhenius plot permits calculating the activation energy (0.28 eV) for the Li_6SiON electrolyte. Table S1 lists the total ionic conductivities of the Li_6SiON electrolyte on Celgard heated to selected temperatures. In comparison, the reported activation energy of amorphous Li_4SiO_4 is 0.62 eV.³⁴

In polymer electrolytes, the anions are typically responsible for ionic conductivity as the cations form a liable bond with

polar groups of the host polymer matrix. Figure 4b shows the two regions for the ionic conductivity vs temperature ($1000/T$) plots, where the ionic conductivity gradually increases ($<25^\circ\text{C}$) and the region where conductivity abruptly increases ($>25^\circ\text{C}$). At high temperatures, the energy is large enough to overcome potential barriers, facilitating the mobility of ionic charge carriers.⁵³

The representative I_{ss} – U relations of Li/ Li_xSiON /Li symmetric cells are shown in Figure 5a–c. As expected from Ohm's law, I_{ss} shows a linear increase with applied potential. The Li_2SiON , Li_4SiON , and Li_6SiON polymer electrolytes exhibit an average electrical conductivity of $2.7 \pm 1.4 \times 10^{-10}$, $6.4 \pm 0.4 \times 10^{-7}$, and $2 \pm 0.1 \times 10^{-6}$ S/cm, respectively, as summarized in Table S2. The electrical conductivity appears to increase with increasing LiNH_2 content, supporting the XPS studies shown in Figure 2b. The electron density seems to increase with increasing added LiNH_2 content, which results in a decrease in binding energy of N 1s.

In addition to the ionic and electrical conductivity, the transference number (t_{Li^+}) is a key factor to evaluate the electrochemical performance of the polymer electrolyte.⁵⁴

Electrolytes with high t_{Li^+} values enable fast charge–discharge capabilities regardless of relatively low ionic conductivities.⁵⁵ Furthermore, electrolytes with high t_{Li^+} values are reported to suppress lithium dendrites and facilitate long cycling with metallic Li anodes.^{56,57} The Nyquist plots of the Li/Celgard+Li_xSiON/Li symmetric cells before and after chronoamperometry measurements at ambient temperature are shown in Figure 6a–c. The Nyquist plots show two semicircles at high and low frequencies attributed to impedance of the polymer electrolytes and solid electrolyte interface (SEI)/charge-transfer resistance at the metallic Li electrode, respectively.

The impedance spectra show that the symmetric cells assembled with Li₂SiON and Li₄SiON electrolytes exhibit low total resistivities after steady-state current. However, the Li/Celgard+Li₆SiON/Li symmetric cells show (Figure 6c) slightly increased resistivity after chronoamperometry measurements. This increase in resistivity is correlated with the formation of an SEI layer and charge-transfer resistance due to the high electrical conductivity of the Li₆SiON polymer electrolyte. Figure 6d–f presents the chronoamperometry plots for the Li/Celgard+Li₆SiON/Li symmetric cells after stabilizing for 1 h. Since the impedances of the polymer electrolytes were lower than the interfacial impedance, the steady-state method used in this work should be considered more of a qualitative than a quantitative study.

The t_{Li^+} values were further confirmed by using data from the DC polarization experiments per eq 3

$$t_{\text{Li}^+} = \sigma_{\text{Li}^+} / (\sigma_e + \sigma_{\text{Li}^+}) \quad (3)$$

where σ_{Li^+} is the ionic conductivity of the polymer electrolytes deduced from the Nyquist plots shown in Figure 3a and σ_e represents the electrical conductivity obtained from the DC polarization studies (Figure 5).

Table 3 summarizes the t_{Li^+} values of the Li_xSiON polymer electrolytes calculated using eqs 1 and 3. The Li–SiON

Table 3. Comparison of t_{Li^+} Calculated Using eqs 1 and 3

sample	t_{Li^+} from eq 1	t_{Li^+} from eq 3
Li ₂ SiON	0.9 ± 0.03	1 ± 0.02
Li ₄ SiON	0.8 ± 0.06	0.79 ± 0.04
Li ₆ SiON	0.73 ± 0.08	0.76 ± 0.06

chemical interaction seems to facilitate a higher Li⁺ mobility as indicated by increased t_{Li^+} for the Li_xSiON polymer electrolytes. In traditional liquid electrolytes and dry solid polymer electrolytes, both the cations and anions are mobile species resulting in a decrease in the t_{Li^+} , which is generally <0.5 due to electropolarization from anion buildup. The electropolarization can lead to a decrease in the overall electrochemical performance due to high internal resistances, voltage losses, and dendrite growth. By anchoring anions to the polymeric backbone, the Li_xSiON polymer electrolytes with t_{Li^+} (~0.75–1) can overcome such challenges as faced by liquid electrolytes.

The calculated t_{Li^+} values for the Li_xSiON electrolytes using both DC polarization and chronoamperometric studies are in good agreement (Table 3). The increase in electrical conductivity results in a relatively lower t_{Li^+} value for the Li₆SiON polymer electrolyte. Studies show that both structural design and material selection can significantly improve the t_{Li^+} values of electrolytes. The migration of anions in polymers can be reduced by anchoring the anions to the polymer backbone or by adding anion receptors that can favorably interact with anions.⁵⁸ The heterojunction and space charge region between the polymer electrolyte and metallic Li electrodes should be studied further to elucidate the ion conduction mechanism and anion mobility.

In addition to t_{Li^+} measurements, electrochemical stability window is an important parameter needed in evaluating the potential stability range for any polymer electrolyte. The electrochemical stability of the Li_xSiON polymer electrolyte was evaluated by assembling a three-electrode half-cell (Li/Celgard+Li_xSiON/SS), where metallic Li was used as both the reference and counter electrodes and SS was used as a working electrode. The electrochemical stability of the polymer electrolyte must be compatible with the operating potential of the electrodes to be considered for practical battery applications. The development of ASSBs with high energy densities strongly relies on the stability of the polymer electrolyte at high potentials.

Figure 7a presents CV plots for the Li/Celgard+Li₆SiON/SS half-cells between potential ranges of –1 to 6 V at 1 mV/sec. Li plating and stripping phenomena are demonstrated by the anodic and cathodic peaks at ~0 V, indicating that the Li⁺ ions diffuse through the polymer electrolyte and plate onto the working electrode. Good electrochemical stability is demon-

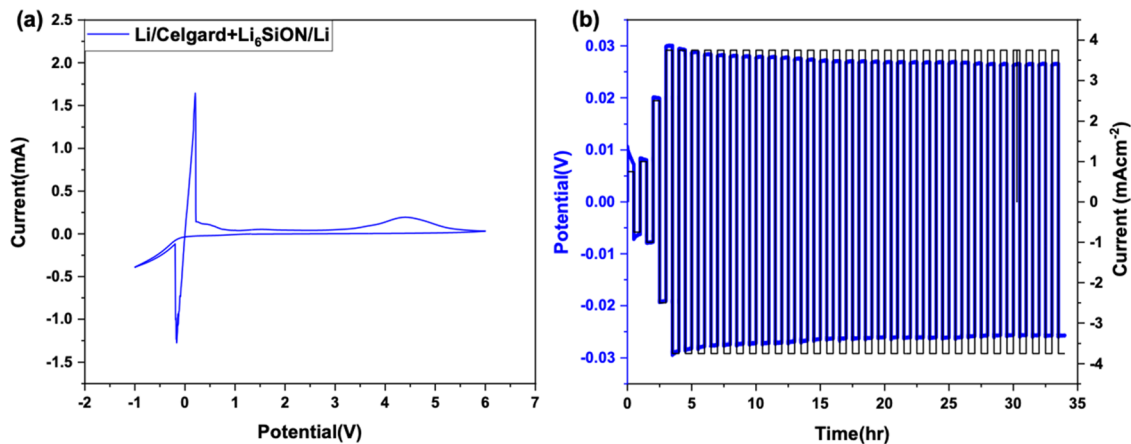


Figure 7. (a) CV plot of Li/Celgard+Li₆SiON/SS at a sweep rate of 1 mV/sec and (b) galvanostatic cycling of Li/Celgard+Li₆SiON/Li symmetric cells at ambient temperature.

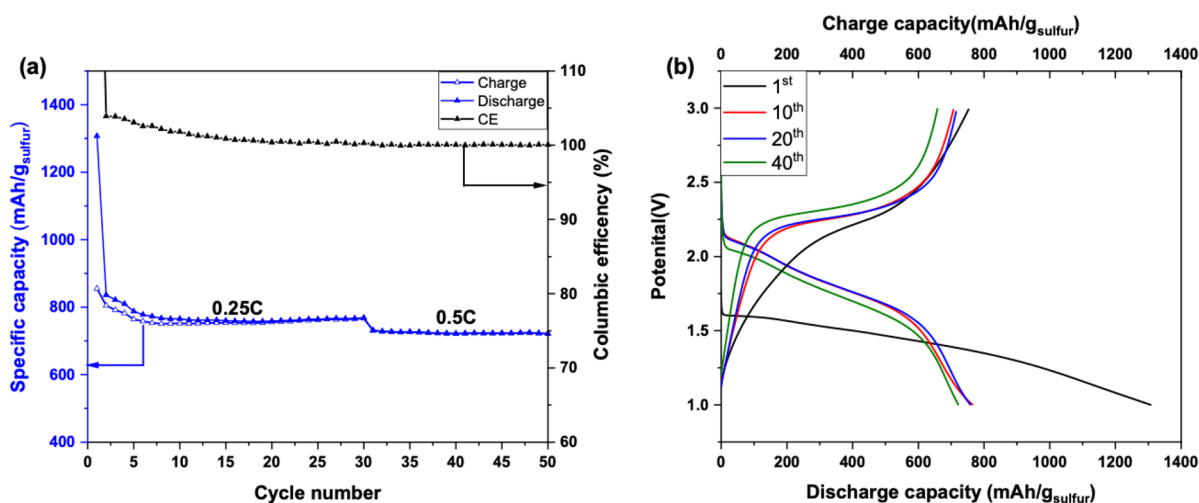


Figure 8. (a) Cycle number vs specific capacity and Coulombic efficiency and (b) potential vs charge/discharge profile at selected cycles for SPAN/Celgard+Li₆SiON/Li half-cells cycled between 1 and 3 V at ambient temperature.

strated by the quite small current response at a high voltage (~ 4.5) vs Li/Li⁺. The current response difference between the polymer electrolyte is attributed to variance in electronegativity of the framework (Figure S1). The increase in Li/Si ratio of the polymer precursor is postulated to decrease the covalency of the Li–N framework, resulting in a decrease in the antibonding energy state.⁵⁹

After investigating the electrochemical stability and transference number of these polymer electrolytes, we now focus on the Li⁺ plating/stripping behavior by charging/discharging the Li/Celgard+Li_xSiON/Li symmetric cells at ambient temperature (Figure S2). Galvanostatic measurements with a constant current density of 0.75–3.75 mA cm⁻² were used to determine the stability of the Li₆SiON polymer electrolyte and Li metal (Figure 7b). The Li/Celgard+Li₆SiON/Li symmetric cell follows ohmic behavior at both low and high critical current densities, delivering an average interfacial resistance of 8 Ω·cm². The voltage response is stable at a high current density of 3.75 mA/cm², meeting the requirement of electrolytes to enable the assembly of ASSBs.^{60,61}

The obtained critical current density for the polymer electrolyte is significantly higher than what is reported for inorganic solid electrolytes with higher ionic conductivities (0.1 mS/cm) at ambient temperature. Irrespective of the use of numerous engineering processes, i.e., polishing, grinding, surface modification, and melting of metallic Li to bind with electrolyte surfaces, voids/pores, grain boundaries, and surface impurities exist in most oxide-based inorganic solid electrolytes.⁴ These surface impurities provide pathways for Li dendrites to penetrate, resulting in low critical current densities (<0.5 mA cm⁻²).⁴

During the past decade, Li–S batteries have drawn intense attention as candidates for next-generation energy storage technologies owing to their high theoretical capacity (1672 mAh/g) and specific energy (2600 Wh/kg).³⁷ Part of the motivation comes from the fact that sulfur is low cost, abundant, and an environmentally friendly resource, making it a very promising cathode material.⁶² Due to its structural framework, SPAN cathodes are known to suppress polysulfide shuttle effects and facilitate fast charging capabilities.

Thus, we investigated the stability of the Li₆SiON electrolyte with a SPAN cathode, metallic Li anode. The current density

and gravimetric capacity were calculated based on the mass of sulfur in the cathode (1 C = 1672 mAh/g = 1 mA/cm²). The half-cell delivered an initial discharge capacity of ~ 1300 mAh/g at ambient temperature (Figure 8a). The reversible capacity was ~ 850 mAh/g at 0.25 C, which gradually decreased to 765 mAh/g after 30 cycles. Fast cycling at 0.5 C resulted in a reversible capacity of 725 mAh/g for the rest of the 20 cycles. The increase in Coulombic efficiency at earlier cycles indicates the formation of side reactions; however, the half-cell maintained a high Coulombic efficiency of $\sim 100\%$ after 15 cycles attributed to the high t_{Li^+} value and optimal ionic conductivity of the Li₆SiON polymer electrolyte. Figure 8b shows the discharge (1.7 V) and charge plateaus (2.2 V) of Li-SPAN half-cells at selected c-rates corresponding to lithiation and delithiation processes, respectively.

4. CONCLUSIONS

We present the detailed electrochemical performance of the Li_xSiON polymer electrolyte, derived from RHA, an agriculture waste product. XRD studies show the amorphous nature of the Li_xSiON polymer electrolyte dried at ambient temperature. The amorphous nature coupled with the high Li and N content resulted in an optimal conductivity of the Li₆SiON electrolyte ($\sim 6.5 \times 10^{-6}$ S/cm) at ambient temperature and low activation energy (0.28 eV). The Li_xSiON polymer electrolytes also exhibit a high Li⁺ transference number (~ 0.7 – 1) attributed to the polymer framework with low anion mobility. The wide electrochemical stability of the Li_xSiON polymer electrolyte makes it attractive for high energy density applications. Most importantly, the polymer electrolyte enabled the assembly of Li symmetric cells with a high critical current density (3.75 mA cm⁻²), making it desirable for fast charging applications. Finally, we assembled half-cells using SPAN as the cathode, Celgard+Li₆SiON as the separator/electrolyte, and Li metal as the anode. The Li-SPAN half-cell delivered a reversible capacity of ~ 725 mAh/g at 0.5 C over 50 cycles.

■ ASSOCIATED CONTENT

Supporting Information

The Supporting Information is available free of charge at <https://pubs.acs.org/doi/10.1021/acsapm.1c00192>.

Supplemental electrical conductivity, ionic conductivity, and symmetrical cell data (PDF)

AUTHOR INFORMATION

Corresponding Author

Richard M. Laine – Dept. of Materials Science and Engineering, University of Michigan, Ann Arbor, Michigan 48109-2136, United States; orcid.org/0000-0003-4939-3514; Email: talsdad@umich.edu

Authors

Eleni Temeche – Dept. of Materials Science and Engineering, University of Michigan, Ann Arbor, Michigan 48109-2136, United States

Xinyu Zhang – Dept. of Materials Science and Engineering, University of Michigan, Ann Arbor, Michigan 48109-2136, United States

Complete contact information is available at: <https://pubs.acs.org/10.1021/acsapm.1c00192>

Author Contributions

The manuscript was written with contributions from all authors.

Notes

The authors declare no competing financial interest.

ACKNOWLEDGMENTS

We are grateful for the support of a significant portion of this work by a gift from Mercedes-Benz Research & Development North America (MBRDNA). A portion of this work was also supported by a DMR NSF grant no. DMR project 1926199. We also like to thank the University of Michigan Rackham Merit Fellowship (RMF) program. We also acknowledge the financial support of the University of Michigan, College of Engineering and NSF grant no. DMR-0402785 (XPS) and technical support from the Michigan Center for Materials Characterization. We also would like to thank Wadham Energy LP for providing the RHA powders. We also thank Zejun Sun, Tianle Liu, and Mengjie Yu for their help in synthesizing SP.

DEDICATION

Dedicated to the memory of Prof. Dr. Andreas Hinntenach, deceased May 10, 2020, as a friend and mentor.

REFERENCES

- (1) Lu, L.; Han, X.; Li, J.; Hua, J.; Ouyang, M. A Review on the Key Issues for Lithium-Ion Battery Management in Electric Vehicles. *J. Power Sources* **2013**, *226*, 272–288.
- (2) Blomgren, G. E. The Development and Future of Lithium Ion Batteries. *J. Electrochem. Soc.* **2017**, *164*, A5019.
- (3) Koga, S.; Krstic, M. Lithium-Ion Batteries. In *Materials Phase Change PDE Control & Estimation*; Birkhäuser: 2020, 199–219, DOI: [10.1007/978-3-030-58490-0_8](https://doi.org/10.1007/978-3-030-58490-0_8).
- (4) Wu, B.; Wang, S.; Evans, W. J., IV; Deng, D. Z.; Yang, J.; Xiao, J. Interfacial Behaviours between Lithium Ion Conductors and Electrode Materials in Various Battery Systems. *J. Mater. Chem. A* **2016**, *4*, 15266–15280.
- (5) Zhou, Q.; Dong, S.; Lv, Z.; Xu, G.; Huang, L.; Wang, Q.; Cui, Z.; Cui, G. A Temperature-Responsive Electrolyte Endowing Superior Safety Characteristic of Lithium Metal Batteries. *Adv. Energy Mater.* **2019**, *10*, 1903441.
- (6) Manthiram, A.; Yu, X.; Wang, S. Lithium Battery Chemistries Enabled by Solid-State Electrolytes. *Nat. Rev. Mater.* **2017**, *2*, 16103.
- (7) Takada, K. Progress and Prospective of Solid-State Lithium Batteries. *Acta Mater.* **2013**, *61*, 759–770.
- (8) Chen, R.; Qu, W.; Guo, X.; Li, L.; Wu, F. The Pursuit of Solid-State Electrolytes for Lithium Batteries: From Comprehensive Insight to Emerging Horizons. *Mater. Horiz.* **2016**, *3*, 487–516.
- (9) Famprikis, T.; Canepa, P.; Dawson, J. A.; Islam, M. S.; Masquelier, C. Fundamentals of Inorganic Solid-State Electrolytes for Batteries. *Nat. Mater.* **2019**, *18*, 1278–1291.
- (10) Zhang, B.; Tan, R.; Yang, L.; Zheng, J.; Zhang, K.; Mo, S.; Lin, Z.; Pan, F. Mechanisms and Properties of Ion-Transport in Inorganic Solid Electrolytes. *Energy Storage Mater.* **2018**, *10*, 139–159.
- (11) Alpen, U. v.; Bell, M. F.; Wichelhaus, W.; Cheung, K. Y.; Dudley, G. J. Ionic Conductivity of $\text{Li}_{14}\text{Zn}(\text{GeO}_4)$ (Lisicon). *Electrochim. Acta* **1978**, *23*, 1395–1397.
- (12) Bruce, P. G.; West, A. R. Ionic Conductivity of LISICON Solid Solutions, $\text{Li}_{2+2x}\text{Zn}_{1-x}\text{GeO}_4$. *J. Solid State Chem.* **1982**, *44*, 354–365.
- (13) Deng, Y.; Eames, C.; Chotard, J.-N.; Lalère, F.; Seznec, V.; Emge, S.; Pecher, O.; Grey, C. P.; Masquelier, C.; Islam, M. S. Structural and Mechanistic Insights into Fast Lithium-Ion Conduction in $\text{Li}_4\text{SiO}_4\text{-Li}_3\text{PO}_4$ Solid Electrolytes. *J. Am. Chem. Soc.* **2015**, *137*, 9136–9145.
- (14) Sakurai, Y.; Sakuda, A.; Hayashi, A.; Tatsumisago, M. Preparation of Amorphous $\text{Li}_4\text{SiO}_4\text{-Li}_3\text{PO}_4$ Thin Films by Pulsed Laser Deposition for All-Solid-State Lithium Secondary Batteries. *Solid State Ionics* **2011**, *182*, 59–63.
- (15) Bachman, J. C.; Muy, S.; Grimaud, A.; Chang, H.-H.; Pour, N.; Lux, S. F.; Paschos, O.; Maglia, F.; Lupart, S.; Lamp, P.; Giordano, L.; Shao-Horn, Y. Inorganic Solid-State Electrolytes for Lithium Batteries: Mechanisms and Properties Governing Ion Conduction. *Chem. Rev.* **2016**, *116*, 140–162.
- (16) Yu, X.; Bates, J. B.; Jellison, G. E.; Hart, F. X. A Stable Thin-Film Lithium Electrolyte: Lithium Phosphorus Oxynitride. *J. Electrochem. Soc.* **1997**, *144*, 524–532.
- (17) Li, J.; Lai, W. Structure and Ionic Conduction Study on Li_3PO_4 and LiPON (Lithium Phosphorous Oxynitride) with the Density-Functional Tight-Binding (DFTB) Method. *Solid State Ionics* **2020**, *351*, 115329.
- (18) Albertus, P.; Babinec, S.; Litzelman, S.; Newman, A. Status and Challenges in Enabling the Lithium Metal Electrode for High-Energy and Low-Cost Rechargeable Batteries. *Nat. Energy* **2018**, *3*, 16–21.
- (19) Bates, J. B.; Dudney, N. J.; Gruzalski, G. R.; Zuhr, R. A.; Choudhury, A.; Luck, C. F.; Robertson, J. D. Electrical Properties of Amorphous Lithium Electrolyte Thin Films. *Solid State Ionics* **1992**, *53-56*, 647–654.
- (20) Lacivita, V.; Westover, A. S.; Kercher, A.; Phillip, N. D.; Yang, G.; Veith, G.; Ceder, G.; Dudney, N. J. Resolving the Amorphous Structure of Lithium Phosphorus Oxynitride (Lipon). *J. Am. Chem. Soc.* **2018**, *140*, 11029–11038.
- (21) Temeche, E.; Zhang, X.; Laine, R. M. Polymer Precursor Derived Li_xPON Electrolytes: Toward Li-S Batteries. *ACS Appl. Mater. Interfaces* **2020**, *12*, 20548–20562.
- (22) Bates, J. B.; Dudney, N. J.; Gruzalski, G. R.; Zuhr, R. A.; Choudhury, A.; Luck, C. F.; Robertson, J. D. Fabrication and Characterization of Amorphous Lithium Electrolyte Thin Films and Rechargeable Thin-Film Batteries. *J. Power Sources* **1993**, *43*, 103–110.
- (23) Lacivita, V.; Artrith, N.; Ceder, G. Structural and Compositional Factors That Control the Li-Ion Conductivity in LiPON Electrolytes. *Chem. Mater.* **2018**, *30*, 7077–7090.
- (24) Zhang, X.; Temeche, E.; Laine, R. M. Design, Synthesis and Characterization of Polymer Precursors to Li_xPON and Li_xSiPON Glasses: Materials That Enable All-Solid-State Batteries (ASBs). *Macromolecules* **2020**, *53*, 2702–2712.
- (25) Bates, J. B.; Dudney, N. J.; Neudecker, B.; Ueda, A.; Evans, C. D. Thin-Film Lithium and Lithium-Ion Batteries. *Solid State Ionics* **2000**, *135*, 33–45.
- (26) Yi, E.; Wang, W.; Mohanty, S.; Kieffer, J.; Tamaki, R.; Laine, R. M. Materials That Can Replace Liquid Electrolytes in Li Batteries: Superionic Conductivities in $\text{Li}_{1.7}\text{Al}_{0.3}\text{Ti}_{1.7}\text{Si}_{0.4}\text{P}_{2.6}\text{O}_{12}$. Processing

Combustion Synthesized Nanopowders to Free Standing Thin Films. *J. Power Sources* **2014**, *269*, 577–588.

(27) Kwon, W. J.; Kim, H.; Jung, K. N.; Cho, W.; Kim, S. H.; Lee, J. W.; Park, M. S. Enhanced Li⁺ Conduction in Perovskite Li_{3-x}La_{2/3-x}□_{1/3-2x}TiO₃ Solid-Electrolytes via Microstructural Engineering. *J. Mater. Chem. A* **2017**, 6257.

(28) Yi, E.; Wang, W.; Kieffer, J.; Laine, R. M. Key Parameters Governing the Densification of Cubic-Li₇La₃Zr₂O₁₂ Li⁺ Conductors. *J. Power Sources* **2017**, *352*, 156–164.

(29) Jung, Y. S.; Oh, D. Y.; Nam, Y. J.; Park, K. H. Issues and Challenges for Bulk-Type All-Solid-State Rechargeable Lithium Batteries Using Sulfide Solid Electrolytes. *Isr. J. Chem.* **2015**, *55*, 472–485.

(30) Luntz, A. C.; Voss, J.; Reuter, K. Interfacial Challenges in Solid-State Li Ion Batteries. *J. Phys. Chem. Lett.* **2015**, 4599–4604.

(31) Haruyama, J.; Sodeyama, K.; Han, L.; Takada, K.; Tateyama, Y. Space-Charge Layer Effect at Interface between Oxide Cathode and Sulfide Electrolyte in All-Solid-State Lithium-Ion Battery. *Chem. Mater.* **2014**, *26*, 4248–4255.

(32) Sharafi, A.; Meyer, H. M.; Nanda, J.; Wolfenstine, J.; Sakamoto, J. Characterizing the Li-Li₇La₃Zr₂O₁₂ Interface Stability and Kinetics as a Function of Temperature and Current Density. *J. Power Sources* **2016**, *302*, 135–139.

(33) Takada, K.; Ohta, N.; Zhang, L.; Fukuda, K.; Sakaguchi, I.; Ma, R.; Osada, M.; Sasaki, T. Interfacial Modification for High-Power Solid-State Lithium Batteries. *Solid State Ionics* **2008**, *179*, 1333–1337.

(34) Nakagawa, A.; Kuwata, N.; Matsuda, Y.; Kawamura, J. Thin Film Lithium Battery Using Stable Solid Electrolyte Li₄SiO₄ Fabricated by PLD. *ECS Trans.* **2010**, *25*, 155.

(35) McCloskey, B. D. Attainable Gravimetric and Volumetric Energy Density of Li-S and Li Ion Battery Cells with Solid Separator-Protected Li Metal Anodes. *J. Phys. Chem. Lett.* **2015**, *6*, 4581–4588.

(36) Zhang, X.; Temeche, E.; Laine, R. M. Li_xSiON (X = 2, 4, 6): A Novel Solid Electrolyte System Derived from Agricultural Waste. *Green Chem.* **2020**, 7491–7505.

(37) Warneke, S.; Zenn, R. K.; Leberherz, T.; Müller, K.; Hintennach, A.; Starke, U.; Dinnebier, R. E.; Buchmeiser, M. R. Hybrid Li/S Battery Based on Dimethyl Trisulfide and Sulfurized Poly-(Acrylonitrile). *Adv. Sustainable Syst.* **2018**, *2*, 1700144.

(38) Warneke, S.; Eusterholz, M.; Zenn, R. K.; Hintennach, A.; Dinnebier, R. E.; Buchmeiser, M. R. Differences in Electrochemistry between Fibrous SPAN and Fibrous S/C Cathodes Relevant to Cycle Stability and Capacity. *J. Electrochem. Soc.* **2017**, *165*, A6017.

(39) Marchal, J. C.; Krug, D. J., III; McDonnell, P.; Sun, K.; Laine, R. M. A Low Cost, Low Energy Route to Solar Grade Silicon from Rice Hull Ash (RHA), a Sustainable Source. *Green Chem.* **2015**, *17*, 3931–3940.

(40) Temeche, E.; Yu, M.; Laine, R. M. Silica Depleted Rice Hull Ash (SDRHA), an Agricultural Waste, as a High-Performance Hybrid Lithium-Ion Capacitor. *Green Chem.* **2020**, *22*, 4656–4668.

(41) Temeche, E.; Zhang, X.; Laine, R. M. Solid Electrolytes for Li-S Batteries: Solid Solutions of Poly(ethylene Oxide) with Li_xPON- and Li_xSiPON-Based Polymers. *ACS Appl. Mater. Interfaces* **2020**, *12*, 30353–30364.

(42) Evans, J.; Vincent, C. A.; Bruce, P. G. Electrochemical Measurement of Transference Numbers in Polymer Electrolytes. *Polymer* **1987**, *28*, 2324–2328.

(43) Nakagawa, A.; Kuwata, N.; Matsuda, Y.; Kawamura, J. Characterization of Stable Solid Electrolyte Lithium Silicate for Thin Film Lithium Battery. *J. Phys. Soc. Jpn.* **2010**, 98–101.

(44) Matanovic, I.; Artyushkova, K.; Strand, M. B.; Dzara, M. J.; Pylypenko, S.; Atanassov, P. Core Level Shifts of Hydrogenated Pyridinic and Pyrrolic Nitrogen in the Nitrogen-Containing Graphene-Based Electrocatalysts: In-Plane vs Edge Defects. *J. Phys. Chem. C* **2016**, *120*, 29225–29232.

(45) Radvanyi, E.; De Vito, E.; Porcher, W.; Jouanneau Si Larbi, S. An XPS/AES Comparative Study of the Surface Behaviour of Nano-

Silicon Anodes for Li-Ion Batteries. *J. Anal. At. Spectrom.* **2014**, *29*, 1120–1131.

(46) Lee, S.-J.; Bae, J.-H.; Lee, H.-W.; Baik, H.-K.; Lee, S.-M. Electrical Conductivity in Li-Si-P-O-N Oxynitride Thin-Films. *J. Power Sources* **2003**, *123*, 61–64.

(47) Kim, Y. G.; Wadley, H. N. G. Lithium Phosphorous Oxynitride Films Synthesized by a Plasma-Assisted Directed Vapor Deposition Approach. *J. Vac. Sci. Technol., A* **2008**, *26*, 174–183.

(48) Zhao, S.; Fu, Z.; Qin, Q. A Solid-State Electrolyte Lithium Phosphorus Oxynitride Film Prepared by Pulsed Laser Deposition. *Thin Solid Films* **2002**, *415*, 108–113.

(49) Lee, S.-J.; Baik, H.-K.; Lee, S.-M. An All-Solid-State Thin Film Battery Using LISIPON Electrolyte and Si-V Negative Electrode Films. *Electrochem. Commun.* **2003**, *5*, 32–35.

(50) Meda, L.; Maxie, E. E. Lipon Thin Films Grown by Plasma-Enhanced Metalorganic Chemical Vapor Deposition in a N₂-H₂-Ar Gas Mixture. *Thin Solid Films* **2012**, *520*, 1799–1803.

(51) Hu, Z.; Li, D.; Xie, K. Influence of Radio Frequency Power on Structure and Ionic Conductivity of LiPON Thin Films. *Bull. Mater. Sci.* **2008**, *31*, 681–686.

(52) Nimisha, C. S.; Rao, K. Y.; Venkatesh, G.; Rao, G. M.; Munichandraiah, N. Sputter Deposited LiPON Thin Films from Powder Target as Electrolyte for Thin Film Battery Applications. *Thin Solid Films* **2011**, *519*, 3401–3406.

(53) Aziz, S. B.; Woo, T. J.; Kadir, M. F. Z.; Ahmed, H. M. A Conceptual Review on Polymer Electrolytes and Ion Transport Models. *J. Sci.: Adv. Mater. Devices* **2018**, *3*, 1–17.

(54) Zheng, Y.; Yao, Y.; Ou, J.; Li, M.; Luo, D.; Dou, H.; Li, Z.; Amine, K.; Yu, A.; Chen, Z. A Review of Composite Solid-State Electrolytes for Lithium Batteries: Fundamentals, Key Materials and Advanced Structures. *Chem. Soc. Rev.* **2020**, 8790.

(55) Kato, Y.; Hori, S.; Saito, T.; Suzuki, K.; Hirayama, M.; Mitsui, A.; Yonemura, M.; Iba, H.; Kanno, R. High-Power All-Solid-State Batteries Using Sulfide Superionic Conductors. *Nat. Energy* **2016**, *1*, 16030.

(56) Shigenobu, K.; Dokko, K.; Watanabe, M.; Ueno, K. Solvent Effects on Li Ion Transference Number and Dynamic Ion Correlations in Glyme- And Sulfolane-Based Molten Li Salt Solvates. *Phys. Chem. Chem. Phys.* **2020**, *22*, 15214–15221.

(57) Lee, Y.-G.; Fujiki, S.; Jung, C.; Suzuki, N.; Yashiro, N.; Omoda, R.; Ko, D. S.; Shiratsuchi, T.; Sugimoto, T.; Ryu, S.; Ku, J. H.; Watanabe, T.; Park, Y.; Aihara, Y.; Im, D.; Han, I. T. High-Energy Long-Cycling All-Solid-State Lithium Metal Batteries Enabled by Silver–Carbon Composite Anodes. *Nat. Energy* **2020**, *5*, 299–308.

(58) Long, L.; Wang, S.; Xiao, M.; Meng, Y. Polymer Electrolytes for Lithium Polymer Batteries. *J. Mater. Chem. A* **2016**, *4*, 10038–10069.

(59) Raj, R.; Wolfenstine, J. Current Limit Diagrams for Dendrite Formation in Solid-State Electrolytes for Li-Ion Batteries. *J. Power Sources* **2017**, *343*, 119–126.

(60) Flatscher, F.; Philipp, M.; Ganschow, S.; Wilkening, H. M. R.; Rettenwander, D. The Natural Critical Current Density Limit for Li₇La₃Zr₂O₁₂ Garnets. *J. Mater. Chem. A* **2020**, *8*, 15782–15788.

(61) Wang, H. C.; Cao, X.; Liu, W.; Sun, X. Research Progress of the Solid State Lithium-Sulfur Batteries. *Front. Energy Res.* **2019**, *7*, 1–20.